The Stirring Tropics. Part I: The Ubiquity of Moisture Modes and Moisture-Vortex Instability

Víctor C. Mayta,[1] Ángel F. Adames Corraliza[1]

Department of Atmospheric and Oceanic Sciences, University of Wisconsin, Madison, Wisconsin

This manuscript was submitted on 03/13/2023 and has not been peer-reviewed.

ABSTRACT: Observations of column water vapor in the tropics show significant variations in space and time, indicating that it is strongly influenced by the passage of weather systems. It is hypothesized that many of the influencing systems are moisture modes, systems whose thermodynamics are governed by moisture. On the basis of four objective criteria, results suggest that all oceanic convectively-coupled tropical depression-like waves (TD-waves) and equatorial Rossby waves are moisture modes. These modes occur where the horizontal column moisture gradient is steep and not where the column water vapor content is high. Despite geographical basic state differences, the moisture modes are driven by the same mechanisms across all basins. The moist static energy (MSE) anomalies propagate westward by horizontal moisture advection by the trade winds. Their growth is determined by the advection of background moisture by the anomalous meridional winds. Radiative heating also maintains their MSE anomalies. Horizontal maps of brightness temperature and 850 hPa streamfunction show that convection is partially collocated with the low-level circulation in nearly all the waves. Both this structure and the process of growth indicate that the moisture modes grow from moisture-vortex instability. Lastly, space-time spectral analysis reveals that column moisture and low-level meridional winds are coherent and exhibit a phasing that is consistent with a poleward latent energy transport. Collectively, these results indicate that moisture modes are ubiquitous across the tropics. That they occur in regions of steep horizontal moisture gradients and grow from moisture-vortex instability suggests that these gradients are inherently unstable and are subject to continuous stirring.

SIGNIFICANCE STATEMENT: Over the tropics, column water vapor has been found to be highly correlated with precipitation, especially in slowly-evolving systems. These observations and theory support the hypothesis that moisture modes exist, a type of precipitating weather system that does not exist in dry theory. In this study, we found that all oceanic tropical depression-like (TD-like) waves and equatorial Rossby waves are moisture modes. These systems exist in regions where moisture varies greatly in space, and they grow by transporting air from the humid areas of the tropics toward their low-pressure center. These results indicate that the climatological-mean distribution of moisture in the tropics is unstable and is subject to stirring by moisture modes.

1. Introduction

The tropical belt (~25°S to 25°N) is characterized by weak spatial and temporal variability of temperature (e.g., Charney 1963; Sobel and Bretherton 2000; Sobel et al. 2001). In contrast, the tropics show a large variability of column water vapor (Fig. 1) that strongly influences the distribution of precipitation (Bretherton et al. 2004). These features lead to one important consequence: the existence of the so-called "moisture modes". Moisture modes can be defined as a type of tropical motion where water vapor plays a central role in its dynamics. The term moisture modes was initially introduced in Yu and Neelin (1994) to refer to a kind of wave characterized by a large humidity signal. The early conception of moisture modes by Sobel et al. (2001) revealed these systems to be akin to Rossby waves that propagate due to the horizontal advection of the background moisture gradient by the anomalous winds. Since the core dynamics of moisture modes lie in the interaction between moisture and convection, they are a type of tropical motion that is distinct from the dry equatorial waves of Matsuno (1966).

With its distinct space-time spectral signature, the Madden-Julian Oscillation (Madden and Julian 1972) was the first tropical phenomenon hypothesized to be a moisture mode (e.g., Raymond and Fuchs 2009; Sobel and Maloney 2012; Adames and Kim 2016; Zhang et al. 2020). The majority of applications of the so-called "moisture mode theory" has since focused on the MJO. More recent studies have suggested that other tropical motions can be moisture modes as well (Gonzalez and Jiang 2019; Adames et al. 2019; Inoue et al. 2020). More recently, Adames (2022) suggested that two types of moisture modes exist: (i) equatorial moisture modes such as the MJO (Raymond et al. 2009; Adames and Kim 2016; Jiang et al. 2018; Zhang et al. 2020) and equatorial Rossby waves (Gonzalez and Jiang 2019; Inoue et al. 2020; Mayta et al. 2022); and (ii) off-equatorial moisture modes such as Pacific easterly waves and monsoon low-pressure systems (Serra et al. 2008; Rydbeck and Maloney 2015; Diaz and Boos 2021).

However, what constitutes a moisture mode? Ahmed et al. (2021) and Mayta et al. (2022) proposed three criteria

Corresponding author: Víctor C. Mayta, mayta@wisc.edu

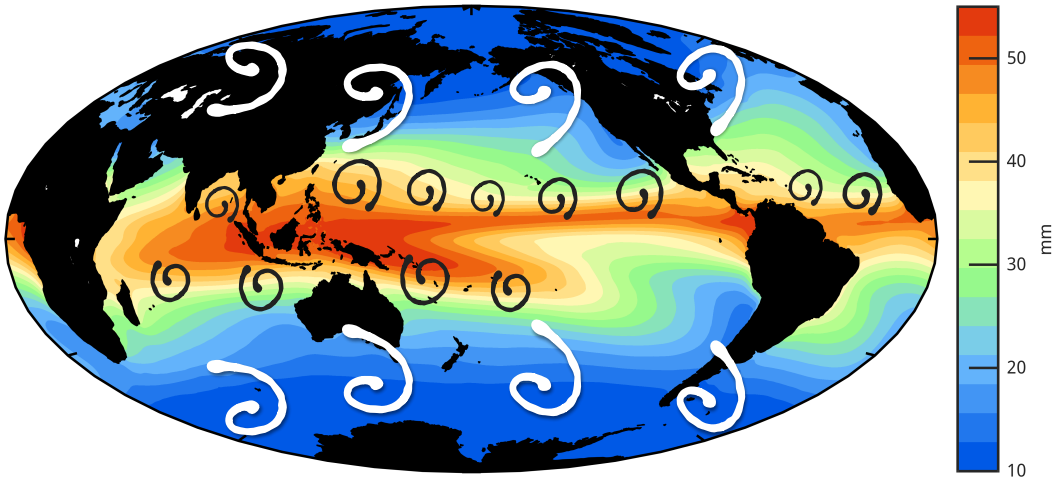

FIG. 1. Annual mean distribution of column-integrated water vapor ($\langle q \rangle$). The black whirls denote tropical eddies that stir column moisture $\langle q \rangle$ in the tropics, behaving as a tropical analog to mid-latitude eddies (white whirls).

to identify moisture modes: their moisture anomalies must dominate the distribution of moist static energy (MSE) and are in phase with the precipitation anomalies, and the thermodynamic equation must be in WTG balance. By using the aforementioned criteria, Mayta et al. (2022) found that moisture modes exist outside the warm pool region. They documented that the slow-propagating equatorial Rossby wave over the Western Hemisphere satisfies all conditions to be considered a moisture mode, in agreement with the scale analysis of Adames (2022). More recently, Mayta and Adames (2023) documented the existence of the second moisture mode over the Western Hemisphere, TD-like waves. The structural features of the Western Hemisphere equatorial Rossby wave are akin to an equatorial moisture mode, while the features of Atlantic TD-like waves are akin to off-equatorial moisture modes.

In the Western Hemisphere equatorial Rossby wave, the trade winds are responsible for the westward propagation of the MSE anomalies. On the other hand, we found that the advection of background-mean MSE by the anomalous meridional winds contributes to the growth of these moisture modes (Mayta et al. 2022). This type of growth was initially documented in the balanced moisture waves of Sobel et al. (2001) and was later referred to as moisture-vortex instability (MVI, Adames and Ming 2018a; Adames 2021). Similar results were found by Gonzalez and Jiang (2019) for western Pacific equatorial Rossby waves. Since MVI only requires a meridional MSE gradient and coupling between moisture and precipitation, it is possible that moisture modes exist in regions where these criteria are met (Fig. 1). This possibility leads to the main questions of this study:

Q1: Are moisture modes common throughout the tropics?

Q2: If so, where are they most common?

Q3: Are the processes that govern the evolution of the Western Hemisphere moisture mode also responsible for the propagation and growth of moisture modes throughout the globe?

The paper is organized as follows. Section 2 provides a brief description of the datasets and analysis methods. In section 3, we elucidate the horizontal structure of TD-like and equatorial Rossby waves and their associated convection on the basis of a linear regression analysis. The governing thermodynamics for all disturbances are examined in section 4. In section 5, an MSE budget analysis is performed for each wave type. The TD-like and equatorial Rossby waves in the wavenumber-frequency domain are assessed in section 6. Finally, a summary and discussion are given in section 7. The major findings of this study are examined within the context of a simple theoretical model in a companion study (Adames-Corraliza and Mayta 2023, hereafter Part II).

2. Data and Methods

a. CLAUS brightness temperature dataset

Satellite-observed brightness temperature (T_b) data is used as a proxy for convection in this study. The data is obtained from the Cloud Archive User System (CLAUS) satellite data (Hodges et al. 2000), which has eight-times-daily global fields of T_b from July 1983 to June 2009 and extended through 2017 using the Merged IR dataset from NOAA.

b. Reanalysis data

To assess the dynamical and thermodynamical characteristics associated with TD-like and equatorial Rossby waves, 4-times daily atmospheric variables from the fifth reanalysis of the European Centre for Medium-Range Weather Forecasts (ECMWF) [ERA5; Hersbach et al. 2019] are used. The ERA5 dataset we employed has a 0.5° horizontal resolution, with four times daily analyses that match the CLAUS T_b data for the 36-yr time period 1984 through 2015. We make use of the zonal (u), meridional (v), and vertical winds (ω), specific humidity (q), temperature (T), apparent heating (Q_1), surface and top of the atmosphere radiative fluxes, surface sensible and latent heat fluxes (SH and L_vE, respectively), and precipitation (P).

c. Wave-type filtering of CLAUS T_b and EOF Calculation

To isolate individual TD-like and equatorial Rossby modes, T_b is filtered following the method proposed by Wheeler and Kiladis (1999) using the same frequency-wavenumber boxes documented in Kiladis et al. (2009). This is accomplished in the wave number-frequency domain by retaining only those spectral coefficients within a specific range corresponding to the spectral peaks associated with TD-like and equatorial Rossby. T_b is filtered using a fast Fourier transform retaining wavenumbers $k = -20$ to 0 and periods between 10 and 96 days for equatorial Rossby waves as in Mayta et al. (2022). For TD-like waves, wavenumbers $k = -20$ to -5 and periods between 2.5 and 10 days are considered.

For the TD-like waves we use a base point to generate an index, while for equatorial Rossby waves the Empirical Orthogonal Function (EOF) analysis is applied to extract the dominant mode associated with the wave as in Mayta et al. (2022). Since T_b are filtered for westward propagation, the EOFs occur in pairs and together account for the leading convective-circulation pattern and propagation. Moreover, the leading two eigenvalues are close together and represent the sine and cosine parts of the wave and they are well-separated from the third eigenvalue based on the North et al. (1982) degenerate mode criteria.

d. Lag regressions

Linear regression is used to examine the evolution of the perturbation convective and dynamical signals over time. To calculate the linear regression, the time series of the corresponding base point for the TD-like waves and principal component (PC) time series for equatorial Rossby is employed. The dynamical fields associated with each corresponding wave are obtained by projecting raw T_b and ERA5 circulation at each grid point onto the associated time series. For TD-like waves, the perturbations are scaled to a -10 K T_b anomaly at the chosen base point, a typical minimum value seen during the convective phase of a TD-like wave. For the equatorial Rossby wave, the dynamical fields associated with each EOF are obtained by projecting unfiltered T_b and ERA5 data at each grid point onto the associated PC time series. Then, all fields are scaled to one standard deviation PC perturbation. The statistical significance of these results is then assessed based on a two-tailed Student's t-test that takes into account the correlation coefficients and an effective number of independent samples (degrees of freedom) based on the decorrelation timescale (Livezey and Chen 1983). Similarly, the governing thermodynamics of these waves are determined by using linear regression, following the same procedure as previous studies (e.g., Kiladis et al. 2006; Adames et al. 2021; Snide et al. 2022; Mayta and Adames 2023).

3. Large-scale features of the TD-like and Equatorial Rossby waves

a. Filtered variance of TD-like waves and Equatorial Rossby waves

Figure 2 shows a map of T_b variance filtered to retain TD-like and equatorial Rossby wave activity only. The variance maps show that the maximum activity of both TD-like and equatorial Rossby waves occurs in off-equatorial regions where the column moisture gradient is steep rather than where column moisture is the largest. Such a result indicates that these waves occur in regions where MVI is possible, a possibility that is examined below. The preference for strong meridional moisture gradients is evident in the correlations between filtered T_b and column moisture and column moisture meridional gradient, respectively, as shown in Table A1.

Based on this variance map, we choose four regions where the T_b variance is a local maximum as base points for the TD-like waves. As shown in Table 1, these regions are located in the Atlantic, eastern Pacific, western Pacific, and the Indian Ocean. For the equatorial Rossby waves, EOF analyses are performed in three regions considering the maximum variance of the equatorial Rossby wave shown in Fig. 2. The regions are the eastern Pacific-Atlantic basin, the western Pacific, and the Indian Ocean (Table 1).

b. TD-like waves across the tropics

Before examining the moist thermodynamics of TD-like waves, we first investigate variations in the TD-like wave life cycle as a function of geographical variations. Figure 3 shows the horizontal structure of the 850-hPa circulation projected onto TD-filtered T_b at different base points. Table 1 summarizes the different base points used over the tropical region based on the maximum variance observed in Fig. 2a.

The base point used for the TD-like wave over the Atlantic region is at 25°W, 7.5°N. The circulation pattern

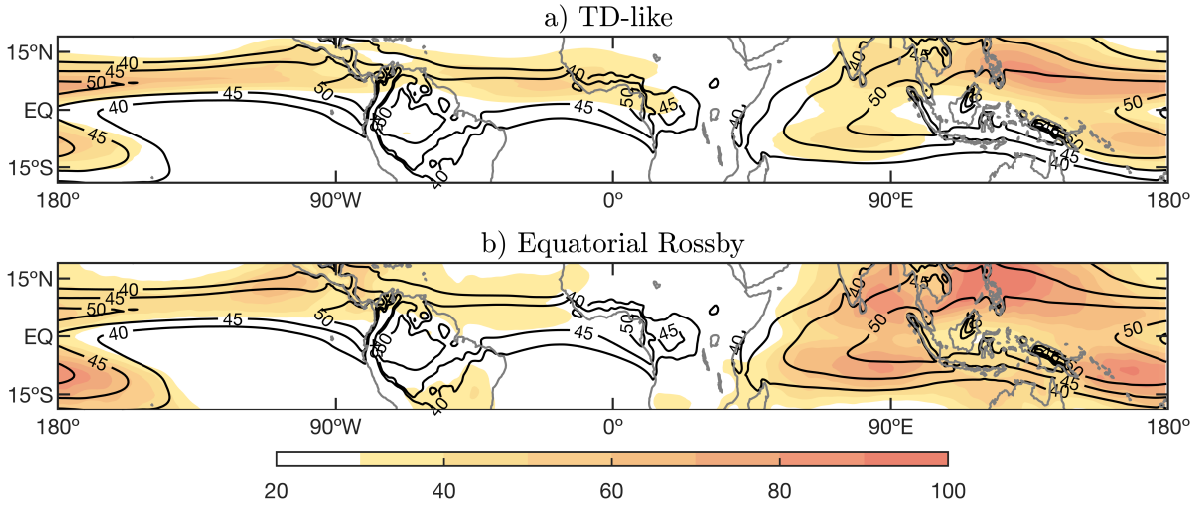

FIG. 2. Geographical distribution of the variance of (a) TD-like and (b) equatorial Rossby wave-filtered CLAUS T_b for all seasons. Shading intervals in K^2 are shown at the bottom of the plot. Contours in both panels indicate the all-season mean of total column water vapor.

TABLE 1. Region chosen for the horizontal and governing thermodynamic analyzes associated with the TD-like and equatorial Rossby waves. For the TD-like waves, the base point corresponds to the maximum variance observed across different ocean basins (Fig. 2a). To investigate equatorial Rossby waves, EOFs are calculated over the region of maximum variance across the tropics (Fig. 2b). The variance explained in % by the two leading patterns (PC1 and PC2) is also shown in the last columns.

Wave	Region	Base point/Domain	PC1	PC2
TD-like	Atlantic [AT]	25°W, 7.5°N	–	–
	Eastern Pacific [EP]	105°W, 10°N	–	–
	Western Pacific [WP]	135°E, 10°N	–	–
	Indian Ocean [IO]	87.5°E, 10°N	–	–
Equatorial Rossby	Atlantic [AT]	5°S–25°N, 125°W–0°	13.4%	12.8%
	Western Pacific [WP]	25°S–25°N, 110°E–150°W	14.7%	11.6%
	Indian Ocean [IO]	20°S–25°N, 50°E–110°E	7.9%	6.9%

associated with this disturbance closely resembles those previously documented over Africa and the Atlantic Ocean (e.g., Kiladis et al. 2006). Over the Atlantic region, these waves propagate at ~ 8.6 m s^{-1}. Similar structure and phase speed were documented recently in Mayta and Adames (2023) by using principal component analysis.

The base point used for regressions of the TD-like wave over the eastern Pacific region is at 105°W, 10°N (Table 1). Despite the circulation and convection evolution being shown for all-year-round, the observed structure closely resembles those Pacific easterly waves documented in many previous works (Serra et al. 2010; Rydbeck and Maloney 2014, 2015; Huaman et al. 2021). Convection moves into the through as the wave propagates toward the west (Fig. 3b). As the waves propagate westward at about 7.3 m s^{-1}, the wave shows the characteristic southwest-northeast tilt, similar to the TD-like waves over the Atlantic region. Such a tilt implies that barotropic energy conversions may play a role in these systems (e.g., Rydbeck and Maloney 2014).

The base point used to explore TD-like activity over the tropical Northwest Pacific is 135°W, 10°N. Fig. 3c shows the characteristic alternating cyclonic and anticyclonic gyres within enhanced and suppressed convection, respectively. Northwestward propagation can be inferred from the equatorial western Pacific toward the Philippines region and southeastern China as documented in previous studies (e.g., Lau and Lau 1990; Kiladis et al. 2009). The wave propagates at about 5.8 m s^{-1}, slightly slower than the TD-like waves over other regions.

The base point used to investigate TD-like activity over the Indian Ocean is 87°W, 10°N. The anomalous anticyclone is followed by cyclonic gyres coupled with enhanced convection (Fig. 3d). The enhanced convection shows its maximum amplitude around the Bay of Bengal and dissipates as the wave propagates toward the west and north at about 7.2 m s^{-1}. The horizontal structure presented in Fig. 3d closely resembles those previously documented for Indian monsoon low-pressure systems (e.g., Hunt et al. 2016; Adames and Ming 2018b; and references therein).

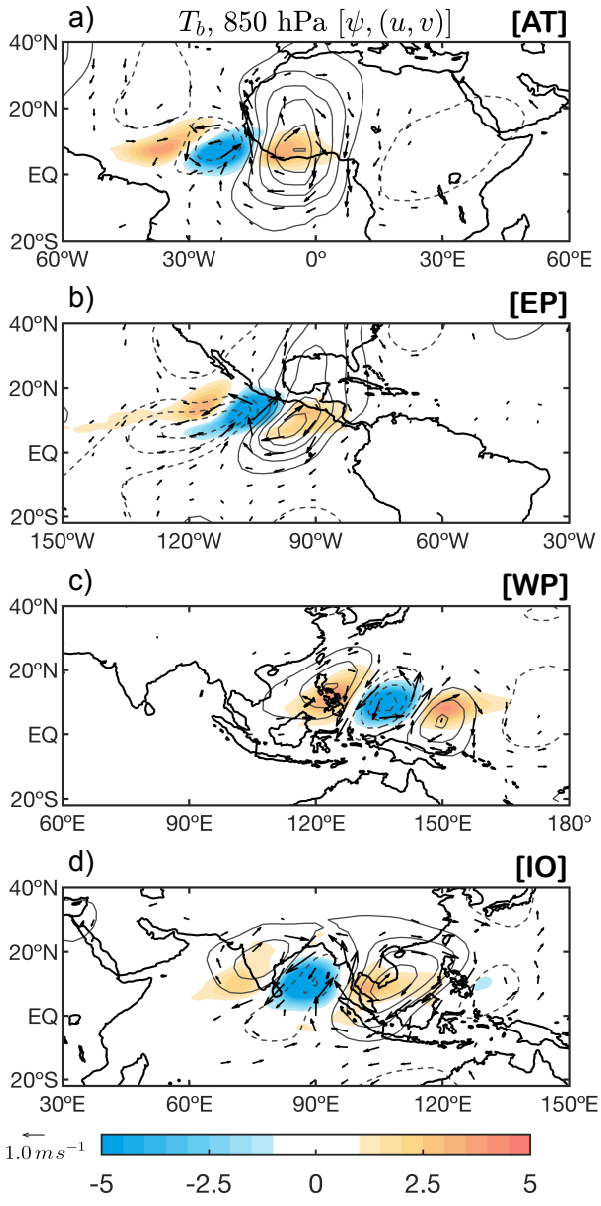

FIG. 3. Anomalous CLAUS T_b (shading), 850 hPa streamfunction (contours), and 850 hPa winds (vectors) regressed onto TD-like wave-filtered T_b at the base point on day 0 in different regions of the tropics: (a) Atlantic ([AT]; 5°S, 7.5°N), (b) Eastern Pacific ([EP]; 105°W, 10°N), (c) Western Pacific ([WP]; 135°E, 10°N), and (d) Indian Ocean ([IO]; 87.5°E, 10°N). All fields are scaled to a -10 K. Streamfunction contour interval is 1.0×10^6 m^2 s^{-1}, with negative contours dashed. Shading and contours indicate regions significant at the 95% level. Wind vectors are plotted only where either the u or v component is significant at the 95% level or greater.

c. *Equatorial Rossby waves across the tropics*

Figures 4a to 4c display the horizontal structure of the 850-hPa circulation projected onto PC1 of the equatorial Rossby wave.

For equatorial Rossby over the Atlantic region, PC1 and PC2 together explain 25% of the filtered variance and represent the equatorial Rossby wave activity over the tropical Atlantic and the Eastern Pacific, in agreement with the geographical distribution of the maximum annual-mean equatorial Rossby variance (Fig. 2b). A detailed description of all features of this wave over the Western Hemisphere is documented in Mayta et al. (2022).

Equatorial Rossby waves over the west Pacific warm pool are presented in Fig. 4b. Over this region PC1 and PC2 together explain 26% of the filtered variance. The predominant zonal wavenumber of the circulation at this level is around k = 4–5. The characteristic cyclonic pair (stronger in the northern hemisphere) is apparent with circulation and convective features propagating westward at a phase speed of 5.9 m s^{-1}. Despite the circulations being more equatorially-trapped like the theoretical wave structure, there is some indication of connections to the extratropics in both hemispheres. Similar features of this wave were documented in previous studies (e.g., Wheeler et al. 2000; Kiladis et al. 2009; Gonzalez and Jiang 2019).

Over the Indian Ocean region, PC1 and PC2 together explain 15% of the filtered variance of the equatorial Rossby wave. Overall, the wave structure varies according to the season (not shown), but Fig. 4c is representative of the annual-mean equatorial Rossby wave. Unlike other tropical regions, the convection and circulation features closely resemble the theoretical Rossby wave structure over the Indian Ocean (Matsuno 1966). A quasi-symmetric pair of cyclonic gyres are clearly visible in Figure 4c. In addition, equatorial easterly wind perturbation to the east of the region of maximum convection resembles the Kelvin response to equatorial heating (Gill 1980). Over the Indian Ocean, equatorial Rossby waves last long enough and propagate slowly at about 3.9 m s^{-1} (Table 3), enough to force a "Gill-type" response, as in the MJO.

4. Governing thermodynamics

In this section, we apply the criteria documented in Adames et al. (2019), Ahmed et al. (2021), and Mayta et al. (2022) to investigate whether all the aforementioned equatorial Rossby and TD-like waves satisfy the conditions to be considered as moisture modes. The four criteria proposed by the authors can be summarized as follows:

a. *Criterion 1 (C1): The wave must exhibit a large moisture signature that is highly correlated with the precipitation anomalies*

For a tropical system to be considered a moisture mode, its signature in column water vapor ($\langle q' \rangle$) must be large enough to significantly modulate surface precipitation (P'). This results in a strong correlation (~0.9 rounded) between P' and $\langle q \rangle'$, because in moisture modes column water vapor should largely explain the rainfall variance, defined

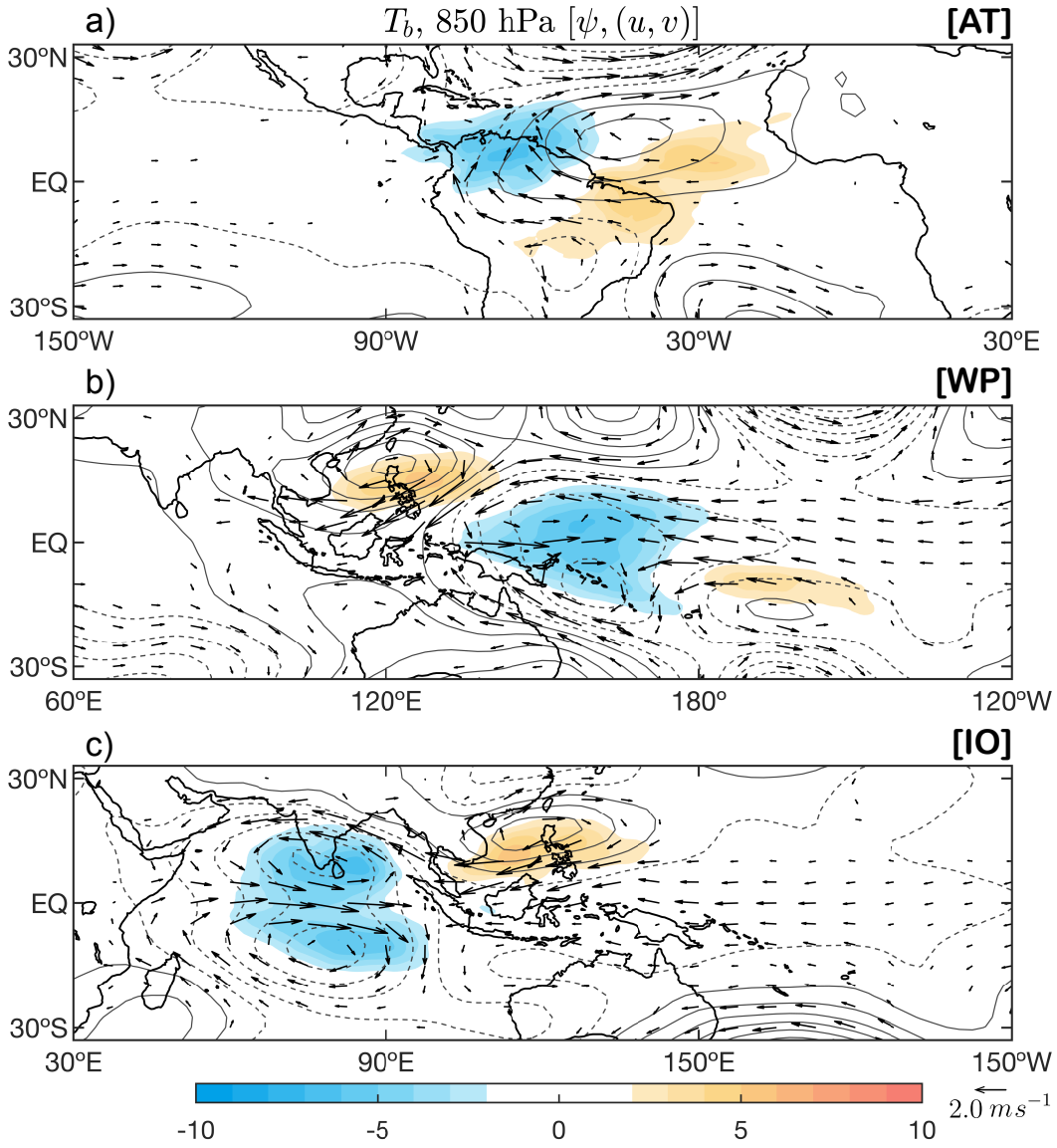

FIG. 4. As in Fig. 3, but regressed onto PC1 equatorial Rossby wave. EOFs were computed in different regions of the tropics: (a) Atlantic ([AT]; 5°S–25°N, 125°W–0°), (b) Western Pacific ([WP]; 25°S–25°N, 110°E–150°W), and (d) Indian Ocean ([IO]; 20°S–25°N, 50°E–110°E). All fields are scaled to one standard deviation PC perturbation of the equatorial Rossby wave. Streamfunction contour interval is 2.0×10^6 m^2 s^{-1}, with negative contours dashed. Shading and contours indicate regions significant at the 95% level. Wind vectors are plotted only where either the u or v component is significant at the 95% level or greater.

as at least 80% in previous studies (Mayta et al. 2022; Mayta and Adames 2023). Previous studies have found that the convective moisture adjustment time scale ($\tau_c = \langle q' \rangle / P'$) varies from 6 to 24 h over the rainy regions of the tropics (e.g., Betts and Miller 1993; Bretherton et al. 2004; Sobel and Maloney 2012; Jiang et al. 2016; Adames and Kim 2016). Thus, Adames et al. (2019) suggested that the τ_c must be larger than 12 h (0.5 days) to guarantee a large moisture signature in moisture modes (see their Fig. 3).

We apply this criterion by constructing a scatterplot between P' and $\langle q \rangle'$ (Figs. 5a, d), where the slope of the linear fit gives the value of τ_c. The τ_c values and the correlation coefficient for TD-like and equatorial Rossby waves over different tropical regions are summarized in Table 2. Results show that TD-like waves pass the first criterion over the entire tropical region, with correlations ranging from ~0.88 to ~0.97 and τ_c larger than 0.5 days. However, there is an exception that occurs with TD-like waves over Africa (i.e., African Easterly waves). As documented re-

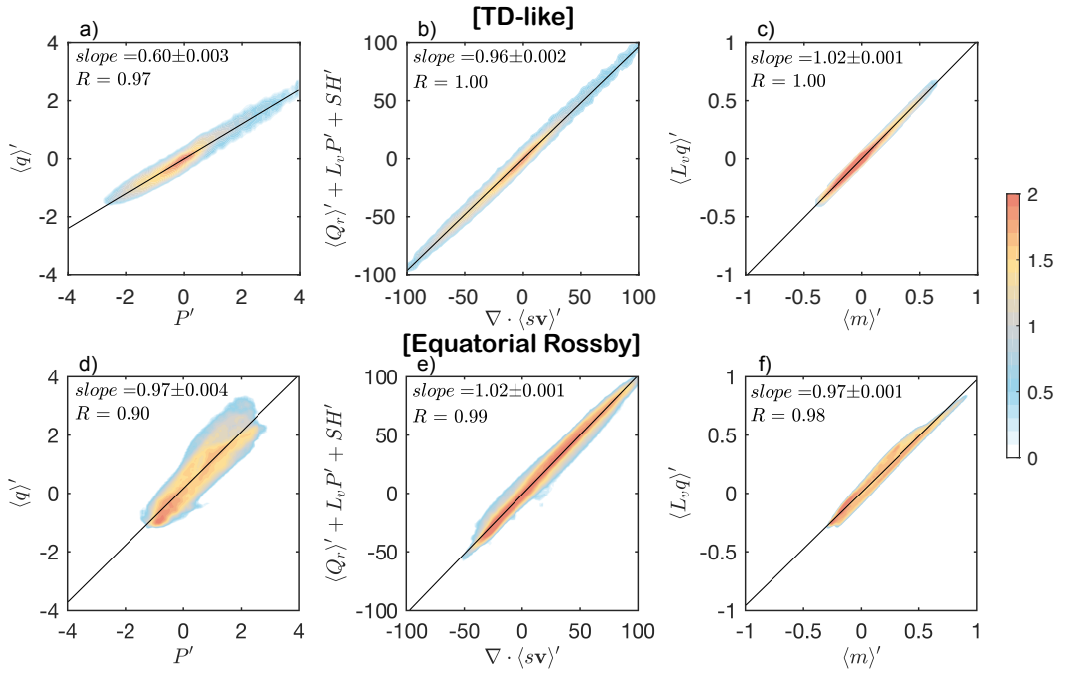

FIG. 5. Scatterplots of (a) P' vs $\langle q \rangle'$, (b) $\nabla \cdot \langle s\mathbf{v} \rangle'$ vs $\langle Q_1 \rangle'$, and (c) $\langle m \rangle'$ vs $\langle L_v q \rangle'$ for the TD-like wave (top) and equatorial Rossby wave (bottom). The shading represents the base-10 logarithm of the number of points within 0.1 mm × 0.1 mm bins in (a), 2.5 W m^{-2} × 2.5 W m^{-2} bins in (b), and 2.0×10^5 J m^{-2} × 2.0×10^5 J m^{-2} bins in (c). Anomalies are obtained by regressing all fields against the TD-like wave filtered T_b at the Western Pacific base point (top); and PC1 (normalized, equatorial Rossby) over the Indian Ocean region (bottom). The domain chosen for the criteria calculation is shown in Table 2. The linear fit obtained from linear least squares fit is shown as a solid black line. The slope of the linear fit and the correlation coefficient are shown in the top-left of each panel.

TABLE 2. Moisture mode criteria applied to TD-like and ER-like waves over different tropical regions. The slope of the linear fit and the correlation coefficient are shown in a similar manner to Fig. 5. * The values for the equatorial Rossby mode over the Atlantic region come from Mayta et al. (2022).

		C1: $P' \propto \langle q \rangle'$		C2: $\nabla \cdot \langle s\mathbf{v} \rangle' \simeq \langle Q_1 \rangle'$		C3: $\langle m \rangle' \approx L_v \langle q \rangle'$	
Wave	Region	Slope	Corr	Slope	Corr	Slope	Corr
TD-like	Atlantic	0.60 ± 0.007	0.88	0.95 ± 0.003	0.99	1.06 ± 0.002	1.00
	Eastern Pacific	0.51 ± 0.003	0.94	0.98 ± 0.002	1.00	1.07 ± 0.003	0.99
	Western Pacific	0.60 ± 0.003	0.97	0.96 ± 0.002	1.00	1.02 ± 0.001	1.00
	Indian Ocean	0.53 ± 0.003	0.90	0.89 ± 0.003	0.97	1.06 ± 0.002	0.99
Equatorial Rossby	E. Pacific - Atlantic*	1.63 ± 0.007	0.96	0.99 ± 0.002	0.99	1.04 ± 0.002	0.99
	Western Pacific	0.91 ± 0.003	0.88	0.98 ± 0.001	1.00	0.89 ± 0.001	0.98
	Indian Ocean	1.04 ± 0.004	0.90	1.02 ± 0.001	0.99	0.97 ± 0.001	0.98

cently in Wolding et al. (2020a) and Vargas-Martes et. al., 2023, temperature fluctuations over these regions are as important as moisture in the thermodynamics of African Easterly waves. Similar results were also found in Mayta and Adames (2023), where a large portion of the TD-like T_b spectrum over the Western Hemisphere (see their Fig. 11) corresponds to the mixed system category of Adames (2022).

The same behavior is found for the equatorial Rossby wave. As observed in Fig. 5d and Table 2, P' and $\langle q \rangle'$ show a strong correlation in all regions ranging from ~0.88 to ~0.96. As also expected, equatorial Rossby waves show slow convective adjustments with τ_c oscillating on order 1.0 days and larger. These values broadly resemble previous findings (e.g., Yasunaga et al. 2019; Adames et al. 2019), where the dominance of moisture ($\tau_c \geqslant 0.5$ days) at low frequencies is found. As documented in Wolding et al. (2020b), small values of τ_c usually mean some other process is causing rainfall, causing τ_c to decrease. In addition, moisture modes rarely exist if the convective adjustment is short (see Ahmed et al. 2021 for more details).

b. Criterion 2 (C2): The wave must satisfy WTG balance at the leading order

The WTG approximation in the column-integrated dry static energy (DSE) budget can be expressed as:

$$\nabla \cdot \langle s\mathbf{v} \rangle' \simeq \langle Q_1 \rangle' \tag{1}$$

where $s = C_p T + \phi$, $\mathbf{v} = u\mathbf{i} + v\mathbf{j}$ is the horizontal vector wind field, and Q_1 is the apparent heating rate. Considering those spatial and temporal variations in temperature are small over tropics, the left hand of Eq. (1) are equivalent to $\omega \partial_p s$. The column-integrated heating can be calculated from ERA5 as follows:

$$\langle Q_1 \rangle' \simeq \langle Q_r \rangle' + L_v P' + SH' \tag{2}$$

where Q_r is the column radiative heating rate, SH is the surface sensible heat flux, and L_v is the latent heat of vaporization (2.5×10^6 J kg $^{-1}$).

To pass this criterion, a wave must exhibit a high correlation (∼0.9 rounded) and the slope must be within the margin of 0.9-1.1 (Mayta et al. 2022). From Fig. 5b, e and Table 2, we can see that the correlation between column DSE divergence and Q_1 is in close unity to all of the TD-like and equatorial Rossby waves. In addition, the slope of the linear least-square fit of the two fields is larger than ∼0.9 in both disturbances.

c. Criterion 3 (C3): Thermodynamic variations in the wave must be dominated by moisture

Moisture modes occur when moisture governs the distributions of anomalous MSE:

$$\langle m \rangle' \approx L_v \langle q \rangle' \tag{3}$$

where $m = s + L_v q$. The same conditions for criterion 2 are used to assess this criterion.

From Fig. 5c, f, we see that the slope of the linear fit is ∼1 for the TD-like and equatorial Rossby waves over the Indian Ocean. It is also satisfied in the other basins studied (Table 2).

When all conditions are examined together, we see that both TD-like and equatorial Rossby waves pass the three criteria across all tropical oceans and hence can be considered moisture modes.

d. N_{mode}

In addition to the three aforementioned criteria, we used the nondimensional number N_{mode} as additional criteria. N_{mode} measures the relative contribution of moisture and temperature in the evolution of moist enthalpy. N_{mode} can be calculated as in Adames et al. (2019):

$$\mathrm{N}_{mode} \simeq \frac{c_p^2 \tau}{c^2 \tau_c} \tag{4}$$

where c is the phase speed of a first baroclinic free gravity wave ($c \simeq 50\, ms^{-1}$), c_p is the phase speed of the wave, τ_c is the convective moisture adjustment time scale, defined as a measure of the sensitivity of precipitation to changes in moisture Betts (1986), and $\tau = \lambda / c_p$ is the temporal time scale with λ being the wavelength. When $\mathrm{N}_{mode} \ll 1$, moisture governs the thermodynamics of a wave, resulting in moisture modes; but if $\mathrm{N}_{mode} \gg 1$ the thermodynamics of a wave are predominantly driven by thermal fluctuations, as in gravity waves. When $\mathrm{N}_{mode} \approx 1$ the wave will exhibit the behavior of both a moisture mode and a gravity wave.

Table 3 shows the values of the parameters in Eq. (4) along with the obtained value of N_{mode}. For the TD-like waves, the largest value of N_{mode} is seen over the Atlantic region, with a value of ≃0.24. Over this region, the wave propagates slightly faster compared to the other regions with a phase speed of ∼8.6 m s^{-1}. TD-like waves over the Eastern Pacific and over the Indian Ocean (Bay of Bengal) show approximately the same N_{mode} value of 0.21 and 0.20, respectively. With a value of 0.13, TD-like waves over the Western Pacific exhibit the lowest value of N_{mode}, largely due to their slower propagation speed of ∼5.8 m s^{-1}. Equatorial Rossby waves, on the other hand, have N_{mode} values that are much smaller than unity ($\mathrm{N}_{mode} \sim$ 0.1) over the three basins assessed in this study. Compared with TD-like waves, equatorial Rossby waves propagate slower at about 4 to 5 m s^{-1}. Over the Western Pacific, the wave propagates slightly fast at 6 m s^{-1}, which results in a larger N_{mode} value of ∼ 0.23 (Table 3).

While the results shown in Table 3 are useful, it is worth mentioning that these values result from a restrictive analysis. To further analyze moisture modes along the tropics, the space-time spectral distribution of N_{mode} is calculated and compared with the typical dispersion curves of convectively coupled equatorial waves, as in Adames (2022) and Mayta and Adames (2023). From an examination of Figure 6 we see that TD-like and equatorial Rossby waves fall well within the moisture mode domain of the N_{mode} spectrum (blue regions). Despite most of the TD-like T_b spectrum falling into the blue region, a portion of the signal falls into the white region that corresponds to mixed systems.

5. MSE Budget Analysis

In the previous section, we demonstrated that moisture modes are common in the tropics. In this section, we employ the column-integrated MSE budget to understand mechanisms associated with the growth and propagation of moisture modes.

The column-integrated MSE budget is defined as in Yanai et al. (1973),

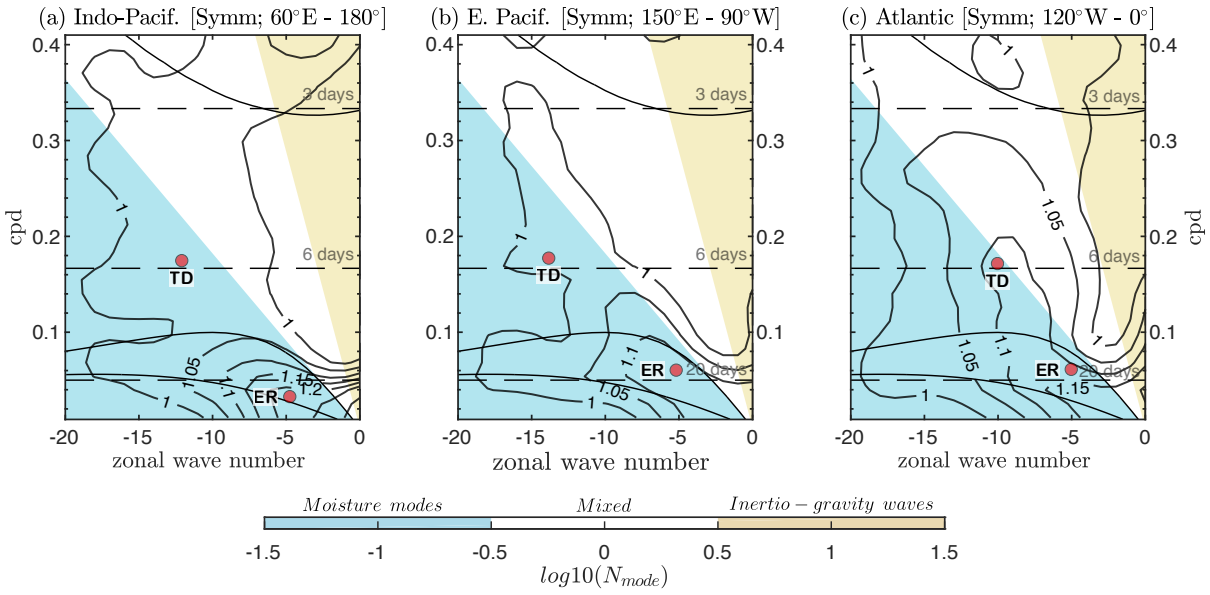

FIG. 6. Regional wavenumber-frequency power spectrum (contours) of the symmetric component of CLAUS T_b calculated for three different regions of the tropics between 10°N–10°S: (a) Indo-Pacific (60°E–180°), (b) Eastern-Pacific (150°E–90°W), and (c) Atlantic (120°W–0°). The solid dispersion curves correspond to 8 and 70 m equivalent depths. The functional form of the tapering window is the same as described in Wheeler and Kiladis (1999). Background spectra were estimated separately for the regional domain, using the smoothing procedure of Dias and Kiladis (2014). Contour interval is 0.05. Shadings represent wavenumber-frequency distribution of base 10 logarithm of N_{mode} following a similar procedure of Adames (2022). Blue shading represents tropical systems that can be categorized as moisture modes, yellow can be considered inertio-gravity waves, and white represents mixed systems. Orange circles approximately represent the average zonal wavenumber and frequency of the corresponding TD-like and Rossby wave for the different regions.

TABLE 3. N_{mode} values for TD-like and Rossby waves. The phase speed (c_p) is calculated by applying a Radon Transform (more details in Mayta et al. 2021 and Mayta and Adames 2021). The convective moisture adjustment time scale (τ_c) is estimated as the slope of the linear fit in the scatterplot of Fig. 5. * The values for the equatorial Rossby mode over the Atlantic region come from Mayta et al. (2022).

Wave	Region	c_p (ms^{-1})	τ (days)	τ_c (days)	N_{mode}
TD-like	Atlantic	8.6	5.2	0.60	0.24
	Eastern Pacific	7.3	5.0	0.51	0.21
	Western Pacific	5.8	6.0	0.60	0.13
	Indian Ocean	7.2	5.2	0.53	0.20
Equatorial Rossby	E. Pacific - Atlantic *	5.4	13.7	1.63	0.10
	Western Pacific	5.9	17.5	0.91	0.23
	Indian Ocean	3.9	24.5	1.04	0.14

$$\frac{\partial \langle m \rangle'}{\partial t} = -\langle \mathbf{v} \cdot \nabla m \rangle' - \left\langle \omega \frac{\partial m}{\partial p} \right\rangle' + \langle Q_r \rangle' + \underbrace{L_v E' + SH'}_{SF'} \quad (5)$$

where $m \equiv s + L_v q$ is MSE. The left-side term in Eq. (5) is the MSE tendency. The first and second terms on the right-side of equation 5 represent horizontal MSE advection and vertical MSE advection, respectively. The other terms on Eq. (5) are MSE source terms: the radiative heating rate, surface latent heat flux ($L_v E$), and surface sensible heat flux. The $L_v E'$ and SH' terms are analyzed together as surface fluxes (SF').

Considering that the horizontal MSE advection governs the propagation and amplification of the slow-moving disturbances (Mayta et al. 2022), we decompose it into the following contributions (Figs. 7 and S5):

$$-\langle u \partial_x m \rangle \approx -\langle \bar{u} \partial_x m' \rangle - \langle u' \partial_x \bar{m} \rangle - \langle u' \partial_x m' \rangle \quad (6a)$$

$$-\langle v \partial_y m \rangle \approx -\langle \bar{v} \partial_y m' \rangle - \langle v' \partial_y \bar{m} \rangle - \langle v' \partial_y m' \rangle \quad (6b)$$

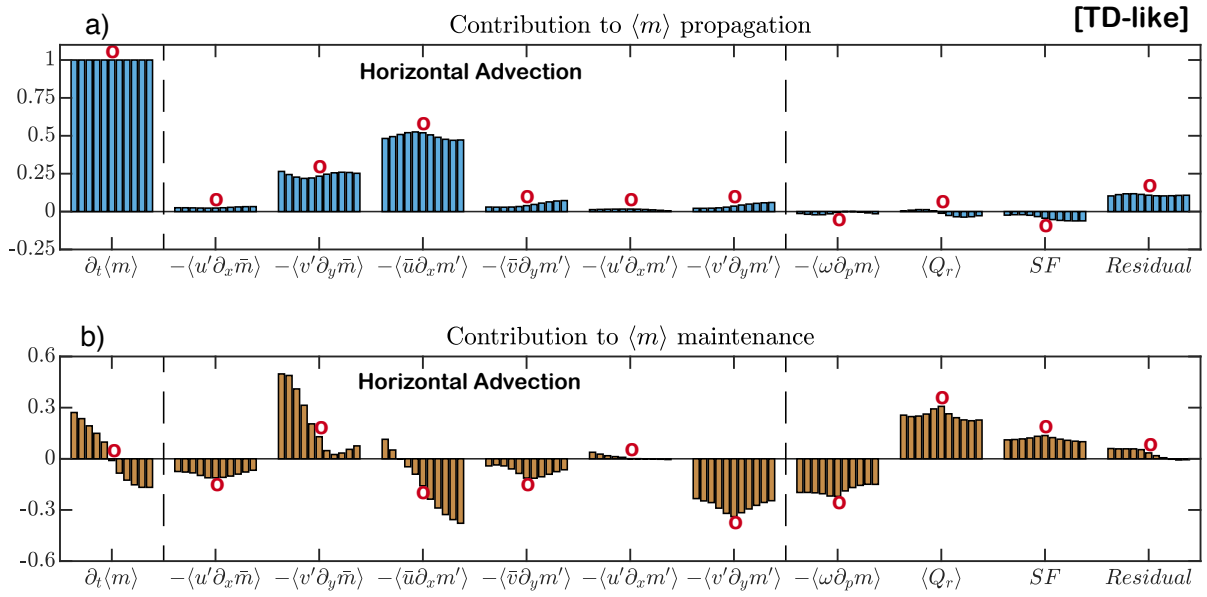

FIG. 7. Normalized contribution of each term in the MSE budget Eq. (5) to the (top) propagation and (bottom) maintenance of the TD-like wave. The contribution of each horizontal MSE advection term is delimited by two dashed black lines in the left part of the panels. Red circles represent the peak of convection at the base point at day 0. The five bins before and after of peak of convection represent the lag regressions from day -2.5 to day +2.5 at every 12 hr.

where the overbar represents the low-frequency component, obtained from a 96-day low-pass filter, and the primes are departures from this low-frequency component for the equatorial Rossby waves. For TD-like waves, we used the same procedure but a 10-day low-pass filter was considered instead.

In addition, following previous studies (e.g., Andersen and Kuang 2012; Arnold et al. 2015; Adames 2017; Mayta and Adames 2023; among others), we estimate the contribution of different processes to the propagation and maintenance of the moisture modes by projecting each MSE budget term upon the MSE tendency and the MSE anomalies, respectively, i.e.,

$$\mathrm{Proj}(F, \partial\langle m\rangle/\partial t) = \frac{||F \cdot \partial\langle m\rangle/\partial t||}{||\partial\langle m\rangle/\partial t \cdot \partial\langle m\rangle/\partial t||} \tag{7a}$$

$$\mathrm{Proj}(F, \langle m\rangle) = \frac{||F \cdot \langle m\rangle||}{||\langle m\rangle \cdot \langle m\rangle||} \tag{7b}$$

where F is each individual term in Eq. (5). $||\cdot||$ implies an areal average from the corresponding lag regressions described in Fig. 7. The lags used for the calculation represent one cycle of the equatorial Rossby and TD-like waves. The area considered for TD-like waves are: 0°–20°N, 80°W–0° [AT]; 0°–20°N, 120°W–80°W [EP]; 0°–20°N, 100°E–180°W [WP], and 0°–20°N, 70°E–100°E [IO]. For the equatorial Rossby waves, we considered the same region used for the EOF calculation detailed in Table 1. The chosen area represents the region where the moisture waves are more active.

Figure 7 shows the average normalized contribution to the propagation and growth of the TD-like waves. Each corresponding basin is displayed in the Supplementary Material (Fig. S1 and S2). This is computed by applying the areal average defined in Eq. (7a) and (7b) to every term in Eq. (5). Each bar represents a time lag, ranging from lag day -2.5 (-8) to 2.5 (8) in TD-like (equatorial Rossby) waves, with the day of maximum wave activity shown as a red circle.

The overwhelming contribution to the MSE tendency for the TD-likes comes from horizontal MSE advection. When we decompose the advection following Eq. (6a) and Eq. (6a). We found that the meridional advection of background MSE by the anomalous winds ($-\langle v'\partial_y\bar{m}\rangle$) and the advection of the MSE anomalies by the mean zonal wind ($-\langle\bar{u}\partial_x m'\rangle$) govern the propagation of the TD-like wave, contributing to over 80% of the column MSE tendency. Other terms contribute little to wave propagation.

As expected for slow-propagating disturbances, one of the largest positive contributors to TD-like growth is the radiative heating $\langle Q_r\rangle'$ (Fig. 7b). Vertical MSE advection ($-\langle\omega\partial_p m\rangle'$) has an opposed and nearly the same magnitude contribution of $\langle Q_r\rangle'$ that approximately cancel each other out, as previous studies have found (Adames and Ming 2018b; Inoue et al. 2020). It is also important to

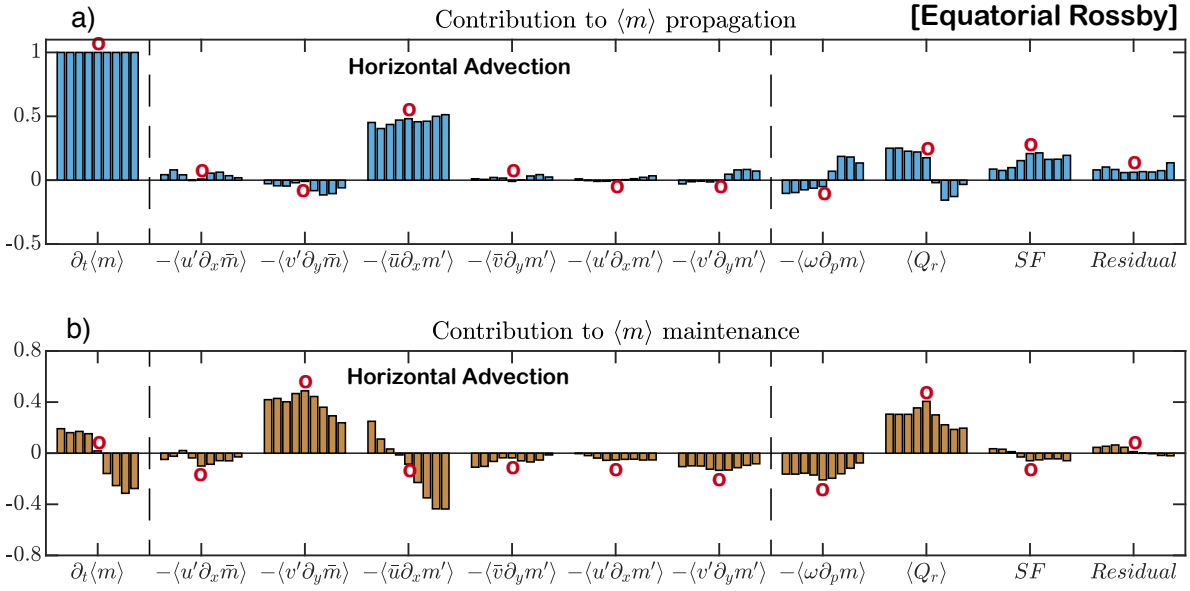

FIG. 8. As in the previous Fig. 7, but for equatorial Rossby waves. The four bins before and after of peak of convection represent the lag regressions from day -8 to day +8 at every 2 days.

note that the growth and decay of the MSE anomalies are largely determined by the horizontal MSE advection. Specifically, it is clear that the meridional moisture advection by anomalous meridional winds ($-\langle v'\partial_y\bar{m}\rangle$) plays a key role in TD-like wave growth (Fig. 7b). In contrast, the term that contributes to the decay of the TD-like wave is $-\langle\bar{u}\partial_x m'\rangle$. TD-like waves over the Atlantic region are one exception (Fig. S2a), where $-\langle\bar{u}\partial_x m'\rangle$ contributes to the growth and decay of the wave before and after the peak of convection, respectively. These results are expected due to differences in the mean state across different basins. Horizontal MSE advection by high-frequency eddies, specifically the meridional component ($-\langle v'\partial_y m'\rangle$), act to dampen the MSE anomalies (Figure 7b).

The processes that propagate and maintain the MSE anomalies in equatorial Rossby waves are similar to those that propagate and maintain the TD-like waves. However, some differences exist in the mechanisms responsible for the propagation of the equatorial Rossby waves. While $-\langle v'\partial_y\bar{m}\rangle$ and $-\langle\bar{u}\partial_x m'\rangle$ propagates the TD-like waves, $-\langle\bar{u}\partial_x m'\rangle$ alone contributes to about 55% of the MSE tendency (Fig. 8a). The same mechanism was recently documented in Mayta et al. (2022), who proposed that the wave propagates westward due to zonal moisture advection by the mean flow. As in TD-like moisture, the major contributors to MSE maintenance are moisture transports by anomalous meridional winds and longwave radiative heating (Fig. 8b). The terms that contribute to the decay of the wave are vertical advection and $-\langle\bar{u}\partial_x m'\rangle$. Only minor differences in these mechanisms are seen across the different basins, as shown in the Supplementary material.

6. Poleward eddy moisture fluxes in moisture modes

That the term $-\langle v'\partial_y\overline{m}\rangle$ acts to amplify the column MSE anomalies in all the waves examined here implies that v' and column water vapor are –at least– partly in phase in these systems. While this phase relationship is consistent with MVI (Adames and Ming 2018a), it also implies that moisture modes flux anomalous moisture poleward (i.e., $\langle v'q'\rangle$ is poleward). In order to examine this possibility, we calculate the space-time spectral coherence and phase angle between 850 hPa v' and $\langle q'\rangle$. Unlike Fig. 6, we will show both eastward and westward-traveling waves and we will examine the northern and southern hemispheres separately. This is done by following the cross-spectral analysis method outlined by Hayashi (1973, 1977). As in Adames et al. (2014) the coherence value at the 99% confidence interval is calculated to be 0.03.

When we examine the coherence squared between v' and $\langle q'\rangle$ (Fig. 9), we see that the most robust coherence values are seen in the westward-propagating moisture mode part of the spectrum in both hemispheres. The northern hemisphere has overall higher coherence values that extend to higher frequencies and zonal wavenumbers, likely due to the higher variance of activity in this hemisphere (see Fig. 2). The phase angle between v' and $\langle q'\rangle$, shown as arrows, reveals that poleward flow is associated with enhanced $\langle q'\rangle$ in both hemispheres. A slight tilt in the arrows– rightward

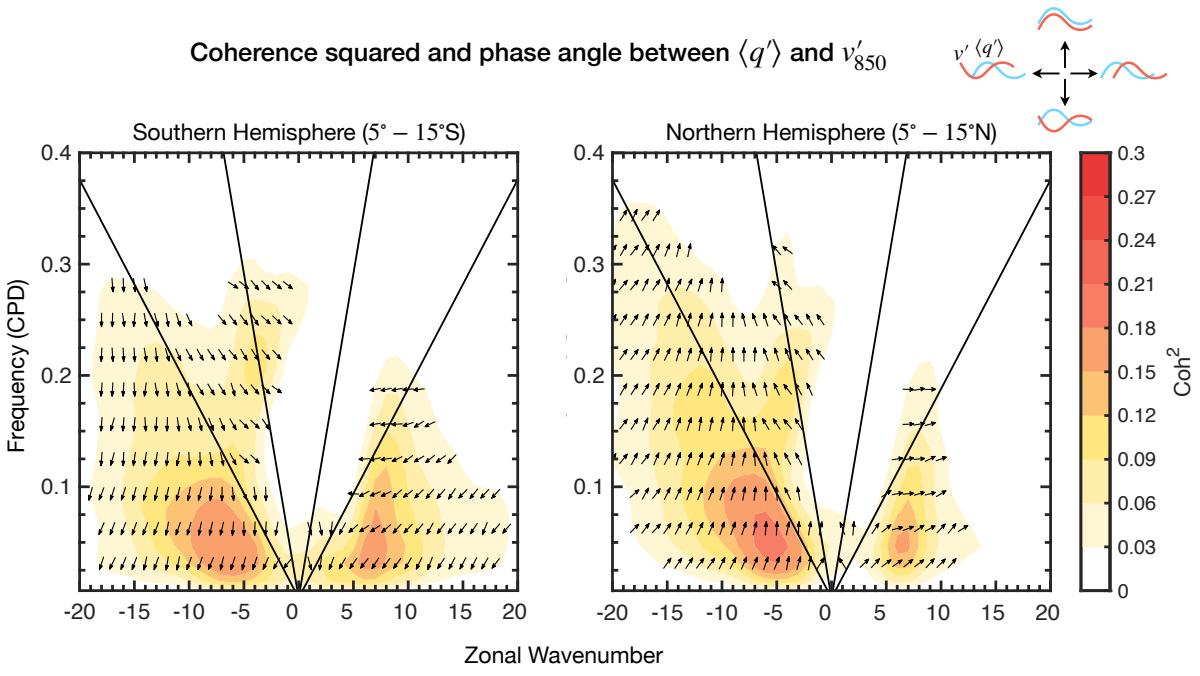

FIG. 9. Coherence squared (shading) and phase angle (vectors) between column moisture ($\langle q' \rangle$) and 850 hPa meridional wind (v'_{850}) for the (left) 5-15°N and (right) 5-15°S latitude belts. In both plots, the solid lines denote the transition lines from moisture modes to mixed systems (lower line) and from a mixed system to gravity wave (top line), as in Fig. 6. A guide to interpreting the phase angle is shown on the top right.

and leftward in the northern and southern hemispheres, respectively – indicates that the poleward flow is shifted eastward from the positive $\langle q' \rangle$ anomalies. This result is consistent with the finding that meridional MSE advection contributes to both the propagation and growth of the MSE anomalies, as shown in Figs. 7 and 8.

The aforementioned results are most robust for the coherence values that are found within the moisture mode region of the spectrum. Closer to the gravity wave part of the spectrum we see a phase angle in the opposite direction. The kink in the spectral signal in this region suggests that the signal here does not correspond to TD-like and equatorial Rossby waves, but rather to mixed-Rossby gravity waves.

We also see a strong coherence in eastward-propagating waves, with the maximum coherence centered near zonal wavenumbers 6-7 in both hemispheres. This signal is akin to the power spectrum found in midlatitude waves (Adames et al. 2014; Tulich and Kiladis 2021). They also transport moisture poleward, but their phase angle is different than those of moisture modes, and their coherence is not as high as those of moisture modes in the latitude belts of interest.

Lastly, it is worth noting that no statistically-significant coherence is seen along the Kelvin wave band or any of the inertio-gravity waves. This result is expected since Kelvin waves do not have a meridional wind signature in the lower troposphere (Kiladis et al. 2009), but it is interesting that little coherence is seen in the gravity waves. It is also intriguing that the coherence between v' and $\langle q' \rangle$ along the MJO band is small.

7. Summary and Conclusions

This study is motivated by increasing evidence that a variety of moisture modes exist within the tropics, even outside of the warm pool, as hypothesized by Adames et al. (2019); Inoue et al. (2020), and Adames et al. (2021). Mayta et al. (2022) found that equatorial Rossby waves over the Western Hemisphere satisfy all criteria to be considered a moisture mode. Mayta and Adames (2023) expanded upon this work and showed that Atlantic TD-like waves also satisfy the criteria to be classified as a moisture mode. Based on these results, we hypothesized that equatorial Rossby waves are equatorial moisture modes and TD-like waves are off equatorial moisture modes as defined by Adames (2022). We examined a series of diagnostic criteria and the governing processes responsible for the growth and propagation of moisture modes by using ERA5 data. To investigate TD-like waves, we chose a base point where the maximum filtered T_b variance was observed. For equatorial Rossby waves, we computed an EOF analysis considering the maximum variance over different tropical regions (see Table 1 and Fig. 10). These indices were used to create lag regressions that elucidated the structure of the waves and their governing thermodynamic processes.

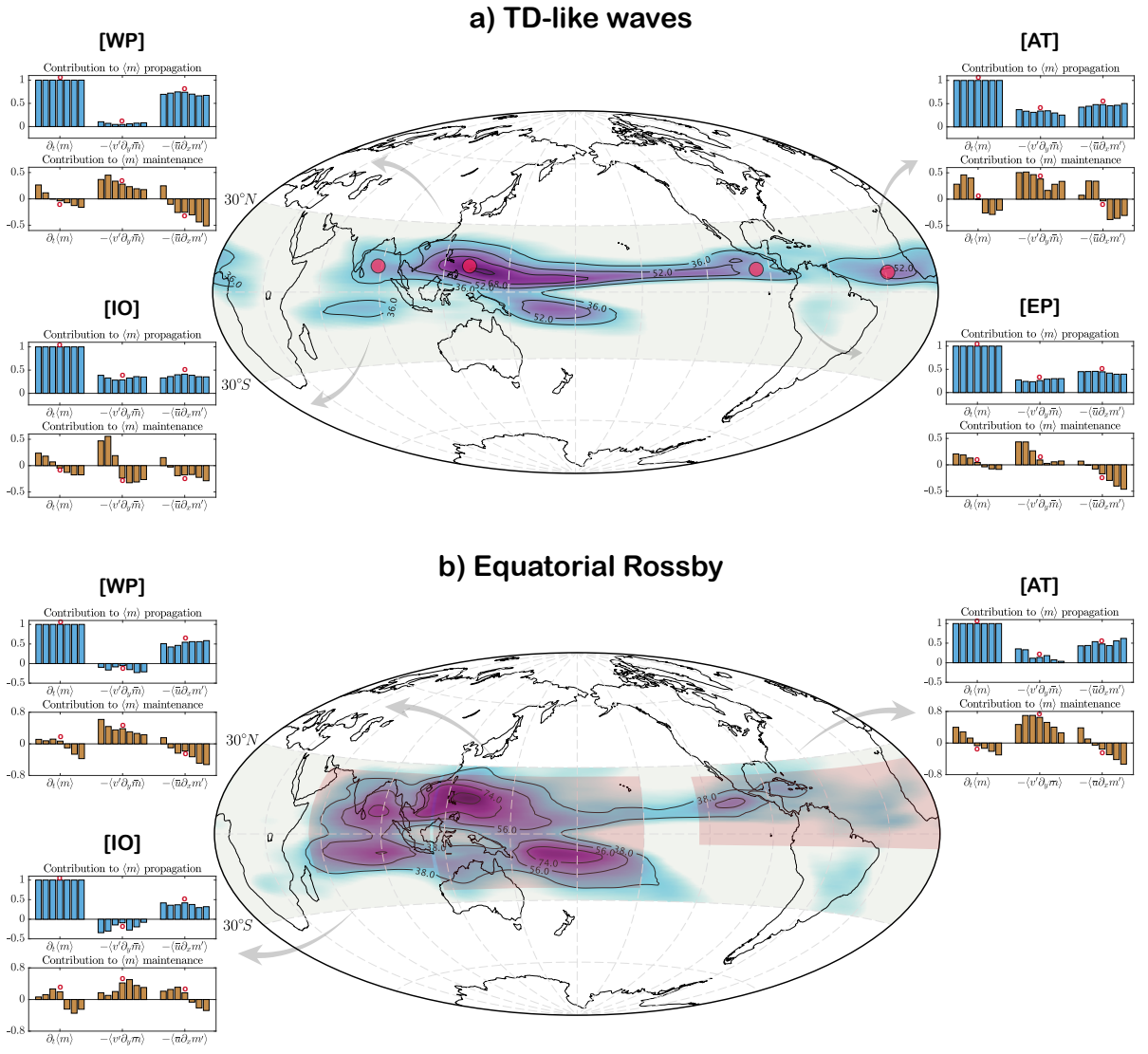

FIG. 10. Schematic depiction that shows the relative contribution of the meridional advection of background MSE by the anomalous winds ($-\langle v'\partial_y \bar{m}\rangle$) and the advection of the MSE anomalies by the mean zonal wind ($-\langle \bar{u}\partial_x m'\rangle$) to the propagation and growth of the MSE anomalies in the (top) TD-like and (bottom) equatorial Rossby waves. Blue and brown bars represent the process responsible for the propagation and maintenance of the moisture modes. The red circles in (a) represent the base point used to explore TD-like waves. The regions considered for the analysis of the equatorial Rossby waves are shown as transparent red polygons (see Table 1 for more details).

The composite dynamical structures, convection, and propagation features of TD-like and equatorial Rossby waves over the entire tropical domain (Figures 3 and 4) depict an evolution that agrees with previous observational studies (e.g., Lau and Lau 1990; Takayabu 1994; Wheeler and Kiladis 1999; Kiladis et al. 2009; Rydbeck and Maloney 2014; Kiladis et al. 2016; Adames and Ming 2018b; Gonzalez and Jiang 2019; Mayta et al. 2022; Mayta and Adames 2023; among others).

By using the four criteria to identify moisture modes, we found that equatorial and off-equatorial moisture modes exist over the whole tropics (Fig. 3 and Table 4). The existence of these two moisture modes was initially predicted by theory (Adames et al. 2019; Adames 2022; Mayta et al. 2022), and their existence was confirmed over the Western Hemisphere (Mayta et al. 2022; Mayta and Adames 2023). Idealized model simulations also found the same results (e.g., Rios-Berrios et al. 2023). These two waves also exhibit an N_{mode} – nondimensional number that measures

the relative contribution of moisture and temperature in the evolution of moist enthalpy (Adames et al. 2019; Adames 2022) – that is much smaller than unity over the entire tropical domain, another requirement necessary to be categorized as a moisture mode (Table 3). These features were also found in the space-time spectral distribution of N_{mode} (Fig. 6). In the three basins considered for the analysis (Indian Ocean-Western Pacific, Central-Eastern Pacific, and Eastern Pacific-Atlantic), the centroid of the TD-like and equatorial Rossby wave signals falls within the moisture mode domain of the spectrum. It is worth noting that, while most of the equatorial Rossby wave signal falls in the moisture mode region, a substantial portion of the TD-like wave signal is outside of this region N_{mode} spectrum (Fig. 6). Thus, not all TD-like waves are moisture modes. Faster-propagating TD-like waves have a larger value of N_{mode} and hence their temperature anomalies are expected to be larger. This is the case seen in African easterly waves, which were recently found to have an N_{mode} value between 0.3-0.5 (Vargas Martes and Adames Corraliza, 2023). Thus, our results indicate that the answer to question 1 in the introduction is:

Q1: Moisture modes are common throughout the tropics.

In addition to the ubiquity of moisture modes found in this study, we also found that the propagation and growth of their MSE anomalies are governed by the same processes (Fig. 10). The propagation of these moisture modes is governed by the advection of the MSE anomalies by the background trade winds, with an additional contribution from advection of background moisture by the anomalous meridional winds. However, in the Indian Ocean equatorial Rossby waves, we found that anomalous surface fluxes contribute non-negligibly to the propagation of the wave, more consistent with the results of Chen (2022).

The growth of the MSE anomalies is the result of the advection of background moisture by the anomalous meridional winds, especially prior to the day in which the moisture modes attain a maximum amplitude. Anomalous radiative heating plays a comparable role in the growth of these moisture modes. Surface fluxes contribute non-negligibly to TD-like waves' growth, which is not seen in equatorial Rossby waves. In contrast, vertical MSE advection dampens the MSE anomalies, and roughly cancels with the radiative heating, in agreement with previous work (Adames and Ming 2018a; Mayta and Adames 2023). Zonal moisture advection by the mean flow contributes to the decay of the wave (Figures 7b and 8b). Lastly, the nonlinear meridional MSE advection term acts to dampen the TD-like waves in all of the regions examined. Equatorial Rossby waves are also damped by the same process but to a lesser extent. It is possible that nonlinear MSE advection may act as a type of diffusion, although more work is needed to better understand this finding.

That the advection of background moisture by the anomalous meridional winds aids in the growth of moisture modes suggests that the MSE anomalies grow from MVI (Sobel et al. 2001; Adames and Ming 2018a; Diaz and Boos 2019; Mayta et al. 2022). This idea is supported by the fact that the highest T_b variance in both equatorial Rossby and TD-like waves is strongest in regions where the horizontal moisture gradient is strong Fig. 2. Furthermore, the horizontal composite maps of T_b and 850 hPa streamfunction of the moisture modes showed that convection is roughly collocated with the cyclonic circulation (Figures 3 and 4). That collocation between circulation and convection is also consistent with MVI (Adames and Ming 2018a).

In light of these findings, our proposed answers to questions 2 and 3 in the introduction are:

Q2: Moisture modes preferentially occur in regions of strong horizontal moisture gradients, suggesting that they grow from MVI.

Q3: Horizontal moisture advection plays a central role in the propagation and growth of all moisture modes. Growth by radiative heating is roughly canceled by damping by vertical MSE advection.

Even though we have answered the three main questions of this study, our results lead to new questions. First, is there a reason why moisture modes appear to be common? Second, why does MVI appear to be so prevalent throughout the tropics? A hint to the answer can be seen in Fig. 9. Since v' and $\langle q' \rangle$ have an in-phase component, then moisture modes have a nonzero $\langle v'q' \rangle$, suggesting that they transport latent energy poleward. This appears to be the case in storm-permitting simulations of the tropics (Rios-Berrios et al. 2020) and even in reanalysis (Trenberth and Stepaniak 2003). Thus, it is possible that moisture modes play an important role in tropical circulation. This possibility will be examined within the context of a simplified model in part II of this study.

8. Data Availability Statement

ERA5 data is available at: `https://www.ecmwf.int/en/forecasts/datasets/reanalysis-datasets/era5/`). Interpolated T_b data are provided by the NOAA/ESRL.

Acknowledgements:

VM and ÁFAC was supported by NSF CAREER grant number 2236433 and by the University of Wisconsin startup package. VM and ÁFAC was also supported by NOAA grant number NA22OAR4310611. We thank George Kiladis for providing us the CLAUS satellite data used in this study. ÁFAC would like to thank his late father, Ángel David Adames Tomassini, for listening to and motivating him to complete this project in spite of strenuous

TABLE A1. Correlation of filtered T_b variance against moisture background ($\langle\bar{q}\rangle$); and meridional gradient of moisture background ($|\partial_y\langle\bar{q}\rangle|$). Correlations are calculated considering different basins based on Figure 2. $|\cdot|$ means absolute value.

Wave	Region	$\langle\bar{q}\rangle \propto T_b$	$\lvert\partial_y\langle\bar{q}\rangle\rvert \propto T_b$
TD-like	Atlantic [AT]	0.44	0.70
	Eastern Pacific [EP]	0.39	0.42
	Western Pacific [WP]	0.38	0.47
	Indian Ocean [IO]	0.50	0.60
Eq. Rossby	Atlantic [AT]	0.28	0.45
	Western Pacific [WP]	0.41	0.32
	Indian Ocean [IO]	0.39	0.51

circumstances. VM also would like to thank Chelsea Snide and the Large-scale Tropical Dynamics Group for helpful discussions throughout the course of this work.

APPENDIX

A1. Is Moisture Mode variance more correlated with the mean moisture or the mean moisture gradient?

In order to explore if strong moisture or meridional moisture plays an important role in the existence of moisture modes, we calculated the correlation between filtered T_b and the annual-mean column moisture and the mean meridional gradient of column moisture. The calculation is made based on Figure 2 and considering different basins. Table A1 summarizes the correlations obtained for both waves over different basins. The results show a stronger correlation between the region of maximum TD-like activity and high values of meridional gradients of moisture background instead of moisture background. The maximum differences in correlations are observed over the Atlantic region and the Indian Ocean with correlations (Table A1) as expected from Figures 1 and 2. The same occurs for the equatorial Rossby waves.

References

Adames, Á. F., 2017: Precipitation Budget of the Madden–Julian Oscillation. *Journal of the Atmospheric Sciences*, **74 (6)**, 1799 – 1817, doi:10.1175/JAS-D-16-0242.1.

Adames, Á. F., 2021: Interactions between water vapor, potential vorticity and vertical wind shear in quasi-geostrophic motions: Implications for rotational tropical motion systems. *Journal of the Atmospheric Sciences*, doi:10.1175/JAS-D-20-0205.1.

Adames, Á. F., 2022: The Basic Equations Under Weak Temperature Gradient Balance: Formulation, Scaling, and Types of Convectively-coupled Motions. *Journal of the Atmospheric Sciences*, **74 (6)**, 1799 – 1817, doi:10.1175/JAS-D-21-0215.1.

Adames, Á. F., and D. Kim, 2016: The MJO as a Dispersive, Convectively Coupled Moisture Wave: Theory and Observations. *Journal of the Atmospheric Sciences*, **73 (3)**, 913 – 941, doi:10.1175/JAS-D-15-0170.1.

Adames, Á. F., D. Kim, S. K. Clark, Y. Ming, and K. Inoue, 2019: Scale Analysis of Moist Thermodynamics in a Simple Model and the Relationship between Moisture Modes and Gravity Waves. *Journal of the Atmospheric Sciences*, **76 (12)**, 3863 – 3881, doi:10.1175/JAS-D-19-0121.1.

Adames, A. F., and Y. Ming, 2018a: Interactions between Water Vapor and Potential Vorticity in Synoptic-Scale Monsoonal Disturbances: Moisture Vortex Instability. *Journal of the Atmospheric Sciences*, **75 (6)**, 2083–2106, doi:10.1175/JAS-D-17-0310.1.

Adames, Á. F., and Y. Ming, 2018b: Moisture and Moist Static Energy Budgets of South Asian Monsoon Low Pressure Systems in GFDL AM4.0. *Journal of the Atmospheric Sciences*, **75 (6)**, 2107 – 2123, doi:10.1175/JAS-D-17-0309.1.

Adames, Á. F., J. Patoux, and R. C. Foster, 2014: The contribution of extratropical waves to the mjo wind field. *Journal of Atmospheric Sciences*, **71 (1)**, 155–176.

Adames, Á. F., S. W. Powell, F. Ahmed, V. C. Mayta, and J. D. Neelin, 2021: Tropical Precipitation Evolution in a Buoyancy-Budget Framework. *Journal of the Atmospheric Sciences*, **78 (2)**, 509 – 528, doi:10.1175/JAS-D-20-0074.1.

Adames-Corraliza, Á. F., and V. C. Mayta, 2023: The Stirring Tropics. Part II: Theory of Wave−Hadley Cell Interactions Mediated By Horizontal Moisture Advection. *Journal of Climate*.

Ahmed, F., J. D. Neelin, and Á. F. Adames, 2021: Quasi-equilibrium and weak temperature gradient balances in an equatorial beta-plane model. *Journal of the Atmospheric Sciences*, **78 (1)**, 209 – 227, doi:10.1175/JAS-D-20-0184.1.

Andersen, J. A., and Z. Kuang, 2012: Moist Static Energy Budget of MJO-like Disturbances in the Atmosphere of a Zonally Symmetric Aquaplanet. *Journal of Climate*, **25 (8)**, 2782 – 2804, doi:10.1175/JCLI-D-11-00168.1.

Arnold, N. P., M. Branson, Z. Kuang, D. A. Randall, and E. Tziperman, 2015: MJO Intensification with Warming in the Superparameterized CESM. *Journal of Climate*, **28 (7)**, 2706 – 2724, doi:10.1175/JCLI-D-14-00494.1.

Betts, A. K., 1986: A new convective adjustment scheme. Part I: Observational and theoretical basis. *Quarterly Journal of the Royal Meteorological Society*, **112 (473)**, 677–691, doi:https://doi.org/10.1002/qj.49711247307.

Betts, A. K., and M. J. Miller, 1993: *The Betts-Miller Scheme*, 107–121. American Meteorological Society, Boston, MA, doi:10.1007/978-1-935704-13-3_9.

Bretherton, C. S., M. E. Peters, and L. E. Back, 2004: Relationships between Water Vapor Path and Precipitation over the Tropical Oceans. *Journal of Climate*, **17 (7)**, 1517–1528, doi:10.1175/1520-0442(2004)017⟨1517:RBWVPA⟩2.0.CO;2.

Charney, J. G., 1963: A Note on Large-Scale Motions in the Tropics. *J. Atmos. Sci.*, **20 (6)**, 607–609.

Chen, G., 2022: A model of the convectively coupled equatorial rossby wave over the indo-pacific warm pool. *Journal of the Atmospheric Sciences*, **79 (9)**, 2267–2283.

Dias, J., and G. N. Kiladis, 2014: Influence of the basic state zonal flow on convectively coupled equatorial waves. *Geophysical Research Letters*, **41 (19)**, 6904–6913, doi:10.1002/2014GL061476, URL http://dx.doi.org/10.1002/2014GL061476.

Diaz, M., and W. R. Boos, 2019: Monsoon depression amplification by moist barotropic instability in a vertically sheared environment. *Quarterly Journal of the Royal Meteorological Society*, **145 (723)**, 2666–2684, doi:10.1002/qj.3585.

Diaz, M., and W. R. Boos, 2021: Evolution of Idealized Vortices in Monsoon-Like Shears: Application to Monsoon Depressions. *Journal of the Atmospheric Sciences*, **78 (4)**, 1207 – 1225, doi:10.1175/JAS-D-20-0286.1.

Gill, A. E., 1980: Some simple solutions for heat-induced tropical circulation. *Quart. J. Roy. Meteor. Soc.*, **106**, 447–462.

Gonzalez, A. O., and X. Jiang, 2019: Distinct propagation characteristics of intraseasonal variability over the tropical west pacific. *Journal of Geophysical Research: Atmospheres*, **124 (10)**, 5332–5351, doi:https://doi.org/10.1029/2018JD029884.

Hayashi, Y., 1973: A method of analyzing transient waves by space-time cross spectra. *Journal of Applied Meteorology and Climatology*, **12 (2)**, 404–408.

Hayashi, Y., 1977: On the coherence between progressive and retrogressive waves and a partition of space-time power spectra into standing and traveling parts. *Journal of Applied Meteorology and Climatology*, **16 (4)**, 368–373.

Hersbach, H., and Coauthors, 2019: Global reanalysis: goodbye era-interim, hello era5. 17–24, doi:10.21957/vf291hehd7.

Hodges, K. I., D. W. Chappell, G. J. Robinson, and G. Yang, 2000: An improved algorithm for generating global window brightness temperatures from multiple satellite infrared imagery. *Journal of Atmospheric and Oceanic Technology*, **17 (10)**, 1296–1312.

Huaman, L., E. D. Maloney, C. Schumacher, and G. N. Kiladis, 2021: Easterly waves in the east pacific during the otrec 2019 field campaign. *Journal of the Atmospheric Sciences*, **78 (12)**, 4071 – 4088, doi:10.1175/JAS-D-21-0128.1.

Hunt, K. M. R., A. G. Turner, P. M. Inness, D. E. Parker, and R. C. Levine, 2016: On the Structure and Dynamics of Indian Monsoon Depressions. *Monthly Weather Review*, **144 (9)**, 3391 – 3416, doi:10.1175/MWR-D-15-0138.1.

Inoue, K., Á. F. Adames, and K. Yasunaga, 2020: Vertical Velocity Profiles in Convectively Coupled Equatorial Waves and MJO: New Diagnoses of Vertical Velocity Profiles in the Wavenumber-Frequency Domain. *Journal of the Atmospheric Sciences*, **77 (6)**, 2139 – 2162, doi:10.1175/JAS-D-19-0209.1.

Jiang, X., M. Zhao, E. D. Maloney, and D. E. Waliser, 2016: Convective moisture adjustment time scale as a key factor in regulating model amplitude of the Madden-Julian Oscillation. *Geophys. Res. Lett.*, **43**, 10,412–10,419.

Jiang, X., Ángel F. Adames, M. Zhao, D. Waliser, and E. Maloney, 2018: A Unified Moisture Mode Framework for Seasonality of the Madden–Julian Oscillation. *Journal of Climate*, **31 (11)**, 4215 – 4224, doi:10.1175/JCLI-D-17-0671.1.

Kiladis, G. N., J. Dias, and M. Gehne, 2016: The Relationship between Equatorial Mixed Rossby–Gravity and Eastward Inertio-Gravity Waves. Part I. *Journal of the Atmospheric Sciences*, **73 (5)**, 2123–2145, doi:10.1175/JAS-D-15-0230.1.

Kiladis, G. N., C. D. Thorncroft, and N. M. J. Hall, 2006: Three-Dimensional Structure and Dynamics of African Easterly Waves. Part I: Observations. *Journal of the Atmospheric Sciences*, **63 (9)**, 2212 – 2230, doi:10.1175/JAS3741.1.

Kiladis, G. N., M. C. Wheeler, P. T. Haertel, K. H. Straub, and P. E. Roundy, 2009: Convectively coupled equatorial waves. *Rev. Geophys.*, **47 (2)**.

Lau, K.-H., and N.-C. Lau, 1990: Observed Structure and Propagation Characteristics of Tropical Summertime Synoptic Scale Disturbances. *Monthly Weather Review*, **118 (9)**, 1888 – 1913, doi:10.1175/1520-0493(1990)118⟨1888:OSAPCO⟩2.0.CO;2.

Livezey, R. E., and W. Y. Chen, 1983: Statistical field significance and its determination by Monte Carlo techniques. *Mon. Wea. Rev.*, **111**, 46–59.

Madden, R. A., and P. R. Julian, 1972: Description of global-scale circulation cells in the tropics with a 40–50 day period. *J. Atmos. Sci.*, **29**, 1109–1123.

Matsuno, T., 1966: Quasi-geostrophic motions in the equatorial area. *Journal of the Meteorological Society of Japan*, **44**, 25–43.

Mayta, V. C., and A. F. Adames, 2021: Two-day Westward-Propagating Inertio-Gravity Waves during GoAmazon. *Journal of the Atmospheric Sciences*, **78 (11)**, 3727–3743, doi:10.1175/JAS-D-20-0358.1.

Mayta, V. C., and Á. F. Adames, 2023: Moist Thermodynamics of Convectively Coupled Waves over the Western Hemisphere. *Journal of Climate*, 1–34, doi:10.1175/JCLI-D-22-0435.1.

Mayta, V. C., Á. F. Adames, and F. Ahmed, 2022: Westward-propagating Moisture Mode over the Tropical Western Hemisphere. *Geophysical Research Letters*, e2022GL097799.

Mayta, V. C., G. N. Kiladis, J. Dias, P. L. S. Dias, and M. Gehne, 2021: Convectively Coupled Kelvin Waves Over Tropical South America. *Journal of Climate*, 1–52, doi:10.1175/JCLI-D-20-0662.1.

North, G. R., T. L. Bell, R. F. Cahalan, and F. J. Moeng, 1982: Sampling errors in the estimation of empirical orthogonal functions. *Mon. Wea. Rev.*, **110**, 699–706.

Raymond, D. J., and Z. Fuchs, 2009: Moisture Modes and the Madden–Julian Oscillation. *Journal of Climate*, **22 (11)**, 3031 – 3046, doi:10.1175/2008JCLI2739.1.

Raymond, D. J., S. L. Sessions, A. H. Sobel, and Z. Fuchs, 2009: The mechanics of gross moist stability. *J. Adv. Model. Earth Syst.*, **1 (9)**, 20 pp.

Rios-Berrios, R., F. Judt, G. Bryan, B. Medeiros, and W. Wang, 2023: Three-Dimensional Structure of Convectively Coupled Equatorial Waves in Aquaplanet Experiments with Resolved or Parameterized Convection. *Journal of Climate*, 1 – 44, doi:10.1175/JCLI-D-22-0422.1.

Rios-Berrios, R., B. Medeiros, and G. H. Bryan, 2020: Mean Climate and Tropical Rainfall Variability in Aquaplanet Simulations Using the Model for Prediction Across Scales-Atmosphere. *Journal of Advances in Modeling Earth Systems*, **12 (10)**, e2020MS002 102, doi:https://doi.org/10.1029/2020MS002102.

Rydbeck, A. V., and E. D. Maloney, 2014: Energetics of east pacific easterly waves during intraseasonal events. *Journal of Climate*, **27 (20)**, 7603 – 7621, doi:10.1175/JCLI-D-14-00211.1.

Rydbeck, A. V., and E. D. Maloney, 2015: On the convective coupling and moisture organization of east pacific easterly waves. *Journal*

of the Atmospheric Sciences, **72 (10)**, 3850 – 3870, doi:10.1175/JAS-D-15-0056.1.

Serra, Y. L., G. N. Kiladis, and M. F. Cronin, 2008: Horizontal and vertical structure of easterly waves in the pacific itcz. *Journal of the Atmospheric Sciences*, **65 (4)**, 1266–1284, doi:10.1175/2007JAS2341.1, URL http://dx.doi.org/10.1175/2007JAS2341.1.

Serra, Y. L., G. N. Kiladis, and K. I. Hodges, 2010: Tracking and Mean Structure of Easterly Waves over the Intra-Americas Sea. *Journal of Climate*, **23 (18)**, 4823–4840, doi:10.1175/2010JCLI3223.1.

Snide, C. E., A. F. Adames, S. W. Powell, and V. C. Mayta, 2022: The role of large-scale moistening by adiabatic lifting in the Madden-Julian Oscillation convective onset. *Journal of Climate*, 269–284, doi:10.1175/JCLI-D-21-0322.1.

Sobel, A., and E. Maloney, 2012: An idealized semi-empirical framework for modeling the Madden-Julian oscillation. *J. Atmos. Sci.*, **69**, 1691–1705.

Sobel, A. H., and C. S. Bretherton, 2000: Modeling Tropical Precipitation in a Single Column. *Journal of Climate*, **13 (24)**, 4378 – 4392, doi:10.1175/1520-0442(2000)013⟨4378:MTPIAS⟩2.0.CO;2.

Sobel, A. H., J. Nilsson, and L. M. Polvani, 2001: The weak temperature gradient approximation and balanced tropical moisture waves. *Journal of the Atmospheric Sciences*, **58 (23)**, 3650 – 3665, doi:10.1175/1520-0469(2001)058⟨3650:TWTGAA⟩2.0.CO;2.

Takayabu, Y. N., 1994: Large-Scale Cloud Disturbances Associated with Equatorial Waves. Part I: Spectral Features of the Cloud Disturbances. *J. Meteor. Soc. Japan*, **72**, 433–449.

Trenberth, K. E., and D. P. Stepaniak, 2003: Covariability of Components of Poleward Atmospheric Energy Transports on Seasonal and Interannual Timescales. *Journal of Climate*, **16 (22)**, 3691 – 3705, doi:https://doi.org/10.1175/1520-0442(2003)016⟨3691:COCOPA⟩2.0.CO;2.

Tulich, S., and G. Kiladis, 2021: On the regionality of moist kelvin waves and the mjo: The critical role of the background zonal flow. *Journal of Advances in Modeling Earth Systems*, **13 (9)**, e2021MS002 528.

Wheeler, M., and G. Kiladis, 1999: Convectively-coupled equatorial waves: Analysis of clouds in the wavenumber-frequency domain. *J. Atmos. Sci.*, **56**, 374–399.

Wheeler, M. C., G. N. Kiladis, and P. J. Webster, 2000: Large-scale dynamical fields associated with convectively coupled equatorial waves. *Journal of the Atmospheric Sciences*, **57 (5)**, 613–640.

Wolding, B., J. Dias, G. Kiladis, F. Ahmed, S. W. Powell, E. Maloney, and M. Branson, 2020a: Interactions between Moisture and Tropical Convection. Part I: The Coevolution of Moisture and Convection. *Journal of the Atmospheric Sciences*, **77 (5)**, 1783–1799, doi:10.1175/JAS-D-19-0225.1.

Wolding, B., J. Dias, G. Kiladis, E. Maloney, and M. Branson, 2020b: Interactions between moisture and tropical convection. Part II: The convective coupling of equatorial waves. *Journal of the Atmospheric Sciences*, **77 (5)**, 1801–1819.

Yanai, M., S. Esbensen, and J.-H. Chu, 1973: Determination of bulk properties of tropical cloud clusters from large-scale heat and moisture budgets. *J. Atmos. Sci*, **30**, 611–627.

Yasunaga, K., S. Yokoi, K. Inoue, and B. E. Mapes, 2019: Space–time spectral analysis of the moist static energy budget equation. *Journal of Climate*, **32 (2)**, 501 – 529, doi:10.1175/JCLI-D-18-0334.1.

Yu, J.-Y., and J. D. Neelin, 1994: Modes of Tropical Variability under Convective Adjustment and the Madden–Julian Oscillation. Part II: Numerical Results. *Journal of the Atmospheric Sciences*, **51 (13)**, 1895–1914, doi:10.1175/1520-0469(1994)051⟨1895:MOTVUC⟩2.0.CO;2.

Zhang, C., Á. F. Adames, B. Khouider, B. Wang, and D. Yang, 2020: Four Theories of the Madden-Julian Oscillation. *Reviews of Geophysics*, **58 (3)**, e2019RG000 685, doi:https://doi.org/10.1029/2019RG000685.